High-Power and Long-Pulse Injection with Negative-Ion-Based Neutral Beam Injectors in Large Helical Device

Y. Takeiri, O. Kaneko, K. Tsumori, Y. Oka, K. Ikeda, M. Osakabe, K. Nagaoka, E. Asano, T. Kondo, M. Sato, M. Shibuya

National Institute for Fusion Science, Toki 509-5292, Japan
e-mail address: takeiri@nifs.ac.jp

Abstract:
A negative-ion-based neutral beam injection (NBI) system has been operated reliably in the Large Helical Device (LHD) since it was operational in 1998. The injection power achieved is 13.1 MW with three injectors. In one injector with modified ion sources with the multi-slotted grounded grid, the injection power reached 5.7 MW with an energy of 184 keV, both of which exceed the designed values of 180 keV - 5 MW. The individual control of the arc-discharge with the divided arc and filament power supplies is effective to improve the beam uniformity. The injection duration is extended to 120 sec with a reduced power of 0.2 - 0.3 MW using one ion source with the cooled plasma grid. The performance of the negative-NBI in LHD is reviewed with regard to the progress of the negative ion sources.

1. Introduction

Neutral beam injection (NBI) heating has been a most reliable and powerful method to heat high-temperature plasmas for fusion plasma research, and the injection energy has increased as the target plasma size has become larger. At higher energy above 100 keV/nucleon, the neutralization efficiency for positive ions decreases drastically while maintaining at around 60 % for negative ions. Therefore, a negative-ion-based NBI system is inevitable for a large-scaled experimental fusion machine such as ITER (International Thermonuclear Experimental Reactor), the injection energy of which is 1 MeV [1]. After 9 years' development of high-current negative ion sources at National Institute for Fusion Science (NIFS) [2-14], a negative-ion-based NBI system started its operation with two injectors in 1998 [15] and the third injector was operational in 2001 [16] in the Large Helical Device (LHD), which is the world's largest superconducting helical system [17]. The LHD negative-NBI system is characterized by a main heating device, in contrast with the JT-60U negative-NBI system for the current drive, which was operational in 1996 [18]. Thus, reliable operation is required for highly repetitive injection in every three minutes. The nominal hydrogen injection energy and power are 180 keV and 5 MW, respectively, for one injector in the LHD-NBI system. The total injection power has been gradually increased year by year [16], and to date has reached up to 13MW. One injector that is equipped with modified ion sources with multi-slotted grounded grid has achieved 184 keV – 5.7 MW injection [19]. On the other hand, two negative-NB injectors can be operated beyond the nominal injection duration of 10 sec, and the injection duration can be extended to several hundreds seconds by reducing the beam energy and power [20]. Using one ion source, a continuous injection for 120 sec was achieved with an injection power of 0.2–0.3 MW.

In this review, we describe the recent injector performance of the LHD negative-NBI system and the characteristics of the high-power negative ion sources. After a brief outline of the LHD-NB injectors and the progress of the high-power injection, large negative ion sources used in the injectors are presented in detail with respects to the structure, negative ion production efficiency, beam acceleration using slotted grounded grid, uniformity, and source lifetime in section 3. The long-pulse injection with the LHD-NBI system is presented in section 4, followed by summary.

2. Negative-NBI System in LHD

Since the Large Helical Device (LHD) has a large major radius of 3.9 m at the helical coil center, the tangential path for a neutral beam injection is long and the required injection beam energy is higher than 120 keV/nucleon for a target plasma density of $1x10^{19}m^{-3}$. At the design of the heating systems, we proposed a negative-ion-based NBI system [21], and started the development of a large negative ion source in 1989. In parallel to the development of the ion source, two negative-NB injectors were constructed in 1995–97 [10]. Using the developed large negative ion sources, we started the injection into the LHD plasma in 1998, and the third injector was operational in 2001. In this section an outline of the LHD negative-NBI system and its injection performance are described.

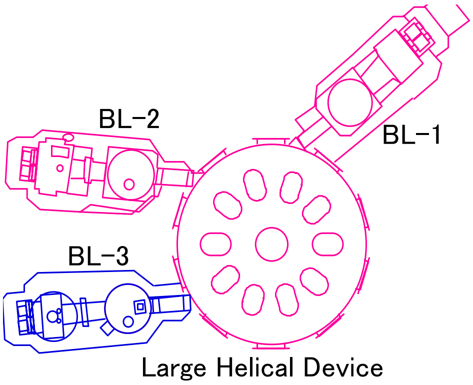

Fig. 1 Arrangement of the negative-ion-based NBI system in LHD.

2.1 Outline of the negative-ion-based injectors

Arrangement of the negative-NBI system in LHD is shown in Fig. 1. Three tangential injectors of BL1, BL2 and BL3 are arranged in which one injector has the opposite injection direction to the other two injectors. The nominal injection energy is 180 keV, and the nominal injection power is 5 MW for one injector. The designed beam duration is 10 sec and the beam species is hydrogen. The injection energy is determined to achieve a high nτT plasma with a target density of around $3x10^{19}$ m^{-3}. Figure 2 shows a schematic diagram of the injector. The injector consists of two large vacuum chambers, the ion source chamber and the beam-dump chamber, which are connected with a neutralizer. Two large negative ion sources are installed side-by-side to the ion source chamber, and the effective neutralization length is 5 m using hydrogen gas. The residual negative and positive ions are magnetically bended and incident on beam-dumps made of swirl tube. A movable calorimeter is located 8.5 m downstream from the ion sources, and the beam profile can be monitored with a thermocouple array. Inner surfaces of the injection port are covered with annularly arranged molybdenum plates, and the port length is about 3 m with the narrowest part of 52 cm in diameter and 68 cm in length. The focal points of multi-beamlets from the ion sources exist inside the narrowest part of the injection port 13 m downstream, and the pivot point is located inside the LHD vacuum vessel 15.4 m downstream from the ion sources. The shine-through beam, passing through the plasma without ionisation, is incident on beam-facing armour tiles installed inside the LHD vacuum vessel. The shine-through power is estimated

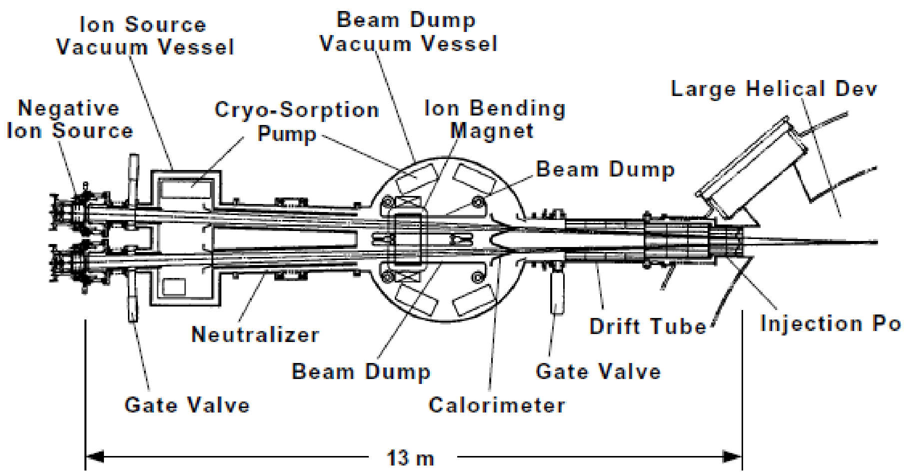

Fig. 2 Plan view of the negative-ion-based NB injector in LHD.

with a calorimeter array on the armour tiles 21 m downstream from the ion sources, and the port-through injection power and the ionization (absorption) power are determined with the shine-through power measurement [22].

In usual plasma experiments, short-pulse injection of around 10 MW of the total injection power is made for 2–3 sec in every 3 min with high reliability. On the other hand, the injection duration can be extended to over 100 sec with a reduced power [23]. The LHD negative-NBI system is a main heating device, and has contributed to the achievement of various plasma parameters in LHD, such as 13 keV of the ion temperature, 4.3 % of the volume-averaged β value, 1.3 MJ of the plasma stored energy, and 2.4×10^{20} m^{-3} of the plasma density [24]. The distinguished result using the LHD-NBI heating is plasma start-up with NBI alone [25]. In many LHD plasma shots especially in low magnetic field experiments in which ECRH (electron cyclotron resonance heating) has no resonant magnetic field, the plasmas are initiated by the NB injection alone and simultaneously heated by the high-power NBI. Thus, the negative-NBI is required to be operated as an indispensable heating system in LHD, and the number of the injection shot is 100 shots a day and summed up to 6000 shots in an experimental campaign for 4 months.

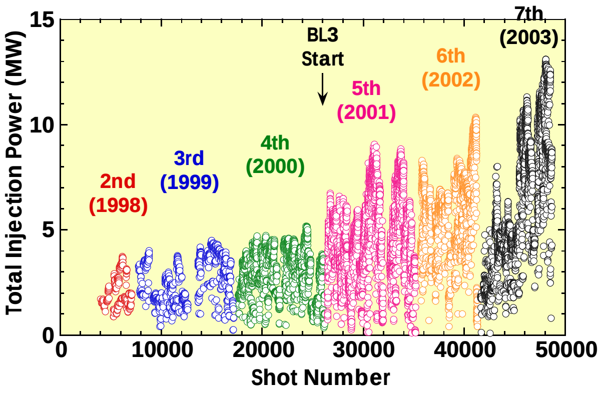

Fig. 3 Progress of the total injection power in the negative-NBI in LHD.

2.2 High-power injection performance

Progress of the total injection power is shown in Fig. 3. The development of the negative ion source has still been continued in parallel with the operation of the LHD-NBI system. The total injection power has gradually increased since the NBI system was first operational in 1998. Except for the increase with the installation of the third injector, the increase in the injection power is mainly due to the improvement of the negative ion sources. Especially, modification of the single-stage accelerator including a change to the multi-slotted grounded grid from the multi-round one has led to a drastic increase in the injection energy and power [26]. The achieved injection energy and power with one injector are 186 keV and 5.7 MW, respectively [19]. The other two injectors has achieved around 4 MW respectively. The maximum total injection power achieved is now 13.1 MW.

3. Powerful Negative Ion Sources

High performance of the negative ion source is essential to high-power and reliable operation of the negative-NBI. The negative ion sources are still under development, and their modification for the improvement is being carried out in the LHD-NBI system. In this section, operational characteristics of the negative ion sources, such as source plasma properties, beam acceleration, beam uniformity, and source lifetime, are presented in detail as well as the source structure.

3.1 Structure of negative ion sources

A schematic diagram of the negative ion source is shown in Fig. 4 [27]. The ion source is a caesium-seeded volume production source equipped with an external magnetic filter, which is developed based on the R&D preceding the construction of the injectors. The arc chamber is rectangular and has large dimensions of 35 cm (width) x 145 cm (length) x 21 cm (depth), which is surrounded by a strong cusp magnetic field of around 2 kG on the inner surface. The external magnetic filter is generated in the width direction as a transverse magnetic field in front of the plasma grid by a pair of permanent magnet rows with a separation of 35 cm. The filter magnetic field strength is 52 G at the centre. Thick tungsten filaments of 1.8 mm in diameter are used for the arc discharge. Three caesium ovens are attached to a back-plate of the arc chamber, and caesium vapour is injected remotely through an air-actuated valve, and the injection rate is controlled with the oven temperature.

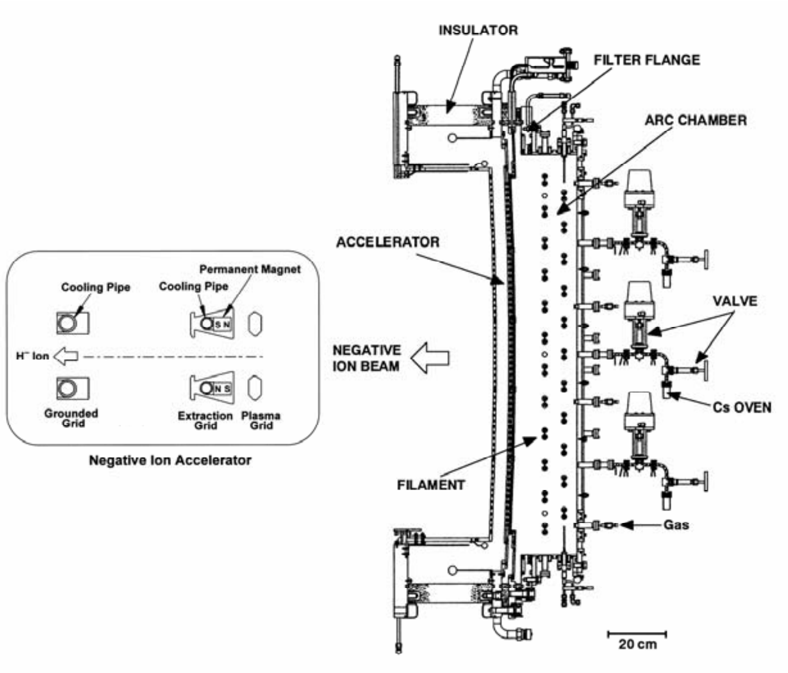

Fig. 4 Schematic diagram of the negative ion source in the LHD negative-NBI.

The negative ion accelerator is a single-stage acceleration system, and originally consists of three grids of plasma grid (PG), extraction grid (EG), and grounded grid (GG). The first gap (PG–EG) and the second gap (EG–GG) are used for beam extraction and acceleration, respectively. The grid area is 25 cm (width) x 125 cm (length), and is segmented into five parts longitudinally, which are jointed so that each part is aimed at a focal point 13 m downstream. Each grid has multi-round apertures in the original source [27], and the GG aperture shape is changed to multi-slotted apertures in the modified source [26]. The PG is made of molybdenum and thermally insulated to keep the PG temperature above 200 ^{o}C for the caesium-seeded operation. The EG contains permanent magnet bars in the width direction for electron suppression, which are buried between the beam aperture rows. The magnetized direction of the magnets is parallel to the beam axis, and the polarity is reversed line by line. The extracted negative ion beamlets are also deflected a little by this magnetic field, and deviate form the aperture centre at the exit of the EG, where the acceleration electric field is applied. As a result, the beamlets are deflected due to the electrostatic lens effect. The deflection direction is reversed line by line, leading to beam expansion as a whole. For compensation of this beamlet deflection, the steering grid (SG), in which the aperture displacement technique is applied for the beamlet steering, is stuck to the exit side of the EG [28,29]. The effectiveness of the SG to the compensation of the beamlet deflection by the EG magnetic field is described in ref. 28 and 29. In order to prevent the secondary electrons generated on the inner surface of the EG apertures from entering the acceleration gap, the EG end aperture is enlarged, and then the narrower aperture of the SG works as a shield against the acceleration electric field, leading to reduction of the electron leakage [11]. In the modified source with the slotted GG, the SG is attached to the EG with a gap for more effective suppression of the secondary electron acceleration [26].

3.2 Efficient negative ion production

In the caesium-seeded negative ion source, the negative ions are produced by conversion of atomic positive ions and neutral atoms on the caesium-covered surface of the PG with a low work function. Thus, high efficiency of the source plasma confinement in the arc chamber is important to produce high density of atomic positive ions, i.e., high density plasma with a high proton ratio. In an external filter source, the magnetic filter is transverse inside the plasma and connected to the strong cusp magnetic field for the plasma confinement. Since strong permanent magnets are used for generation of the magnetic filter, local connection of the filter field with the cusp field could result in plasma loss and plasma localization. The filament positions also influence the arc discharge characteristics. To optimize the configuration of the confinement magnetic field from a point of view of the combination of the magnetic filter field and the cusp field, the orbit calculation of primary electrons emitted from the filaments is carried out. Figures 5 (a) and (b) show calculation results of the distribution of the primary electrons emitted from filaments for a non-optimized and an optimized field configurations, respectively. In the non-optimized configuration, since a part of the filter field is strongly connected with the cusp magnetic field on the side wall, some primary electrons are locally trapped at mirror fields near the wall, and contribute hardly to the efficient plasma production. On the other hand, the filter field is formed almost independently of the cusp field in the optimized configuration, where the cross-sectional shape of the arc chamber is modified hexagonal so that the local connection of the filter field with the cusp magnetic field is reduced. As a result, a uniform distribution of the primary electrons is realized in the driver region, leading to improvement of the plasma production efficiency. The upgrade of the arc chamber was made based on this optimization to improve the negative ion production efficiency. Comparison of the arc efficiency, defined as a ratio of the negative ion current to the arc power, is shown in Fig. 6, between the non-optimized and the optimized arc chambers shown in Fig. 5. It is found that the arc efficiency is much improved by the field optimization. The operational gas pressure can be lowered even at high arc power in the optimized configuration. In the optimized arc chamber, the correlation of the negative ion current to the arc power is not linear because the operational condition, such as the plasma grid temperature and the balance of the individual arc currents that are described later, is selected for a high-current operation higher than 30 A. The design of the magnetic field configuration for the filter field

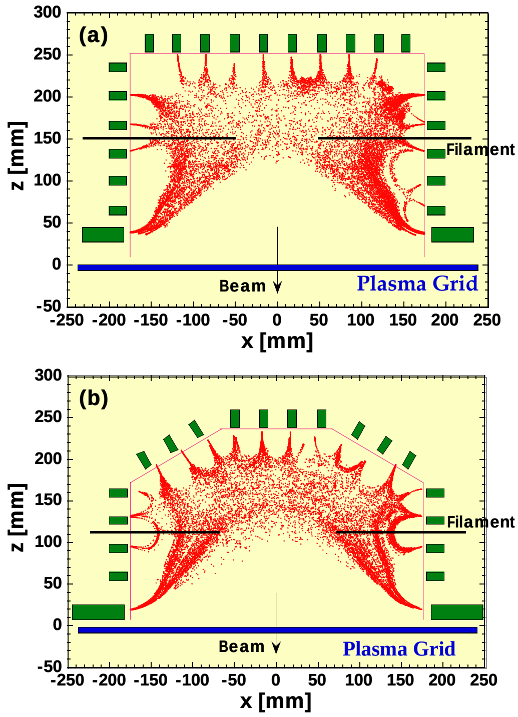

Fig. 5 Calculation results of primary electron distribution in the arc chamber for (a) a non-optimized field configuration and (b) an optimized field configuration.

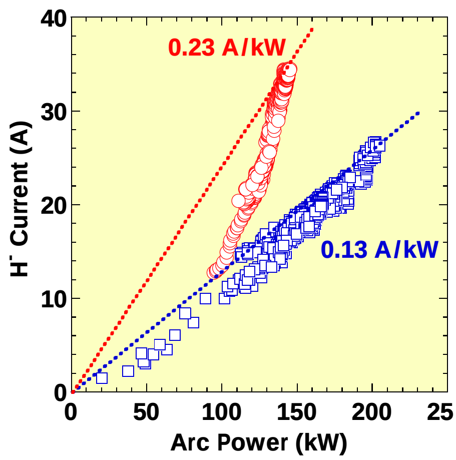

Fig. 6 H^- ion current as a function of the arc power for the non-optimized arc chamber and the optimized arc chamber.

and the cusp field is important to efficient negative ion production at lower operational gas pressure.

3.3 Beam acceleration with slotted GG

The negative ion acceleration is accompanied inevitably by the electron acceleration. Most of secondary electrons generated inside the EG aperture are suppressed with the combination of the EG aperture shape and the SG, which is described in section 3.1. The stripped electrons generated with neutralization of the negative ions by collision with the background gas are incident on the GG surface, resulting in heat load of the GG. High heat- load of the GG would cause out gas, which enhances the stripping loss of negative ions. The ionization of the background gas by the accelerated negative ions and electrons is also enhanced with the out gas. The direct intersection of the negative ions with the GG contributes to the heat load and, moreover, leads to the secondary ion emission, in which the emitted ions are accelerated upstream. These processes cause the breakdown at the acceleration gap frequently. Higher transparency of the GG would be effective to reduction of the gas pressure in the acceleration gap and to reduction of the GG heat load. Thus, we have modified the GG aperture structure from multi-round apertures to multi-slotted apertures to raise the GG transparency. Figure 7 shows a schematic diagram of the modified accelerator with the multi-slotted GG. The transparency is increased by a factor of about 2 in the multi-slotted GG, compared with the multi-round GG. As for the beamlet steering for the multi-beamlet focusing in the horizontal direction along the slot, the aperture displacement technique is applied to the steering grid (SG), and the amount of the displacement is added to that for the compensation of the beamlet deflection by the EG magnetic field. For the multi-beamlet focusing in the vertical direction perpendicular to the slot, the aperture displacement technique is applied to both the SG and the GG. While it takes a long conditioning period of about 1 month to raise the beam energy to a maximum value of 165 keV in the original GG with multi-round apertures, the conditioning period has been much shortened to about 1 week and the beam energy has reached the design value of 180 keV in the modified GG with multi-slotted apertures.

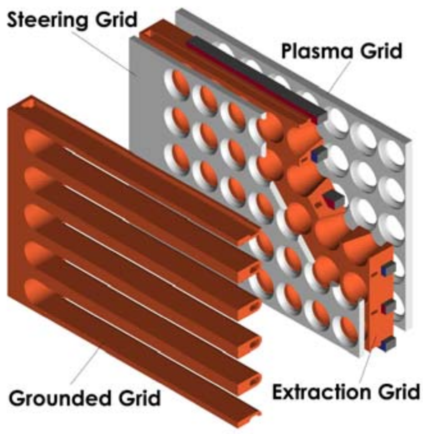

Fig. 7 Schematic diagram of the modified accelerator with the multi-slotted grounded grid.

The heat load of the GG as a function of the supplied energy of the acceleration power supply is shown in Fig. 8, for the multi-round GG and the multi-slotted GG. It is found that the GG heat load is reduced to about a half in the multi-slotted GG compared with that in the multi-round GG. Since the transparency is 2 times higher in the multi-slotted GG, the electron and ion beam intersection area is reduced. The gas pressure in the acceleration gap is calculated to be lowered by a factor of 2.5, and then the stripping loss is estimated to be reduced to about a half. Therefore, due to both the reduction of the beam intersection area and the reduction of the stripping loss, the GG heat load is much reduced, resulting in the quick raise and the enhancement of the beam energy.

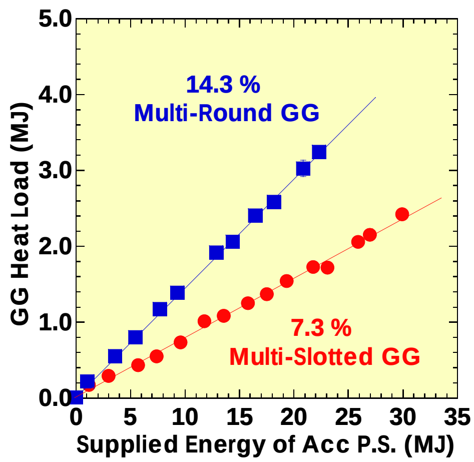

Fig. 8 Heat Load of the grounded grid (GG) as a function of the supplied energy of the acceleration power supply for the multi-round GG and the multi-slotted GG.

The injection power is proportional to the 5/2 power of the beam energy as shown in Fig. 9. In the multi-round GG source, the injection power was less than 4 MW, and was limited by the voltage holding for the beam energy of less than 165 keV. In the multi-slotted GG source, the beam energy can be raised beyond the design value of 180 keV due to the improvement of voltage holding ability, which is accompanied by an increase in the negative ion current according to the 3/2 power law of the beam energy with the optimized arc chamber described in the previous sub-section. The injection power using two ion sources has been increased up to 5.7 MW at a beam energy of 184 keV without a saturation.

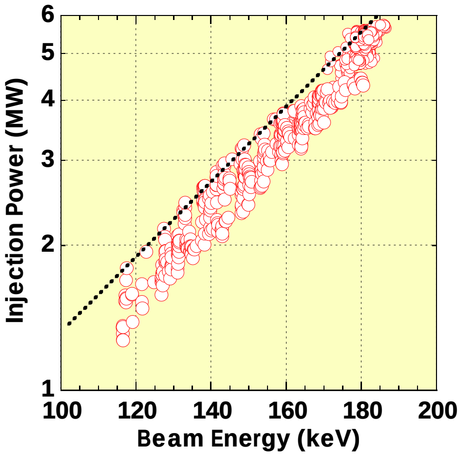

Fig. 9 Injection power into the LHD as a function of the beam energy using one injector with the modified ion sources with the multi-slotted GG.

The SG and GG apertures work as a convergence lens and a divergence lens, respectively, for the acceleration electric field. The electrostatic lens effect in the direction perpendicular to slots is larger than that in a round aperture, and there is no lens effect along slots except for the slot edge. As a result, an optimum condition to give a minimum divergence is different between the perpendicular and the parallel directions to the GG slots, and the perpendicular divergence is larger. Figure 10 shows the beam widths perpendicular and parallel to the slots measured on the calorimeter 8.5 m downstream from the ion source with a focal length of 13 m. The beam widths are plotted as a function of the electric field ratio of the acceleration to the extraction, and the optimum electric field ratio is larger for the perpendicular width to the slots than that for the parallel one. In the actual injection condition, the field ratio is determined at an intermediate value of the optimum values giving the minimum perpendicular and parallel divergences so that the port-through efficiency of the injected beam is maximized. However, the perpendicular divergence angle seems to be larger than the design value of 10 mrad, and a part of the injection port corresponding to the rectangular beam corners is heated up to a high-temperature due to the vertically diverged injection beam. The divergence angles of the injection beam are roughly estimated at 8 mrad and 16 mrad for the horizontal (parallel to the slots) and vertical (perpendicular to the slots) directions, respectively, from the profiles on the calorimeter and on the beam facing armour 21 m downstream from the ion source located inside the LHD vacuum vessel. For reducing the perpendicular divergence and lowering the deference of the optimum field ratio for the perpendicular and the parallel divergence, the aperture shape of the SG has been changed to a race track shape or an ellipse shape from a round shape to adjust the different lens effects in the perpendicular and the parallel directions at the slotted GG. Since these shapes of the SG aperture correspond to the different lens effects to the parallel and the perpendicular directions at the slotted GG, it is expected that the anisotropic

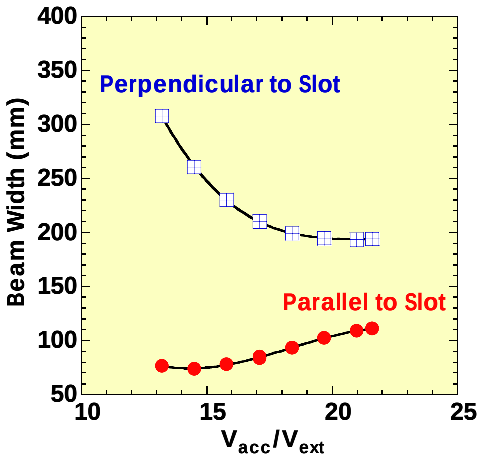

Fig. 10 Beam width in the directions perpendicular and parallel to the slotted direction as a function of the ratio of the acceleration voltage to the extraction voltage in the modified accelerator with the multi-slotted GG.

properties of the perpendicular and the parallel divergence should be compensated. Now, optimization of the method is tested, and the results are presented elsewhere.

3.4 Beam uniformity and PG temperature control

The source plasma uniformity is closely related to the beam uniformity. In the negative ion source, since the filter magnetic field is transverse inside the large and slender arc chamber, the arc discharge tends to be localized, leading to a non-uniform distribution of the produced plasma along the perpendicular direction to the filter field. To improve the plasma uniformity, the output of the arc power supply is divided into twelve circuits, each of which is connected to an electrically insulated filament power supply, and the individual control of the arc discharge is carried out with the divided circuits. The individual output resistances of the twelve arc circuits have been adjusted to control the corresponding 12 arc circuit currents. This method is effective to a uniform plasma production [27]. However, as the arc-plasma uniformity is sensitive to the discharge power distribution and the caesium condition, it would be better to adjust the individual arc discharges directly and remotely with the output voltages of the divided arc circuits. The individual control of the applied voltage to the filaments should also be effective to improvement of the arc-plasma uniformity. In the third injector, both outputs of the filament and the arc power supplies are divided into 12 circuits, respectively, and the individual output voltage of each divided power supply is controlled independently and remotely [29,30]. Figure 11 (a) shows vertical distribution of the individual applied voltages of the arc and the filament power supplies. Filaments are attached to the side wall of the vertically elongated arc chamber, and 24 filaments are usually used. Two filaments located at the same vertical height, which face each other in the filter field direction, are heated in parallel by one electrically insulated filament power supply, which is connected to a divided output of the arc power supply. When the same arc voltage is applied to the 12 output circuits, the distribution of the individual arc currents is not uniform at all with a variation of a factor of 3 - 5. By controlling the individual arc voltages together with the individual filament voltages as shown in Fig. 11 (a), the arc current distribution becomes uniform. As a result, the vertical distribution of the arc-discharge power is uniform, as shown in Fig. 11 (b). The arc-discharge power distribution should correspond to the plasma uniformity. Figure 11 (c) shows the vertical profile of the negative ion beam measured on the calorimeter 8.5 m downstream from the ion source. In the figure, the calculated profile, in the case of a uniform

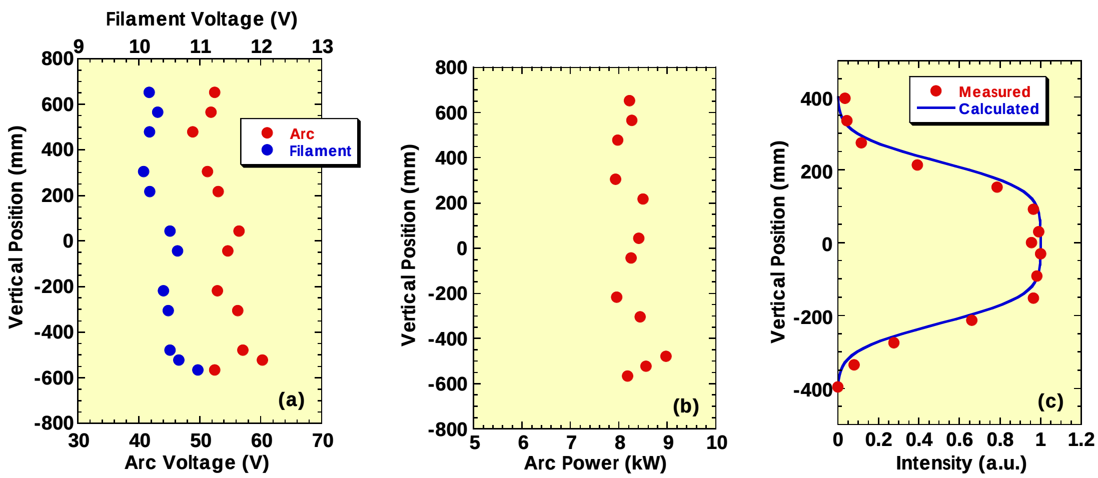

Fig. 11 Vertical distribution of (a) the individual applied voltages of the arc and the filament power supplies and (b) the individual arc-discharge power. The vertical profile of the negative ion beam measured on the calorimeter 8.5 m downstream from the ion source. The calculated profile for a uniform beam with a divergence angle of 10 mrad is also shown by a solid line in the figure.

beam production with a divergence angle of 10 mrad, is also indicated by a solid line. The measured profile corresponds well to the calculated profile, indicating a uniform beam production. The individual control of both the arc voltage and the filament voltage is effective to the uniform beam production from a slender arc chamber of 35cm x 145cm with the external magnetic filter..

Control of the PG temperature for the segmented parts is also important to improve the beam uniformity. The negative ion production efficiency is sensitive to the caesium coverage on the PG surface, which is influenced by the PG temperature. The PG is thermally insulated to such an extent as maintaining the appropriate PG temperature, and all segmented parts are not necessarily maintained at the same temperature because the heat removal from the PG between shots is dependent on the extent of thermal contact with the grid support. Although the arc distribution has an influence on the PG temperature distribution, adjustment of the thermal contact in the individual PG parts leads to an improvement of the beam uniformity. In the cooled PG for long-pulse operation, a uniform beam is obtained, and the detail is shown in section 4.

3.5 Cs consumption and filament lifetime

Most of the introduced caesium is deposited on cold surfaces such as the arc chamber surface, and a part of it escapes from the arc chamber through the PG aperture after the end of discharge. As the deposited caesium is re-evaporated and recycled in the next discharge, the escaping caesium is counted as a loss. The caesium deposited away from the discharge region would not be recycled and is also counted as a loss. Since the contaminated caesium has no effect to the negative ion production, it is regarded as a loss, and tungsten vapour from the filaments could be one of the main contaminants. The introduced caesium from the ovens, which corresponds to the caesium consumption for the source operation, is estimated with measurement of the caesium oven weight loss [31]. Although the Cs consumption rate varies with the operational condition, the Cs oven weight loss was 14 - 15 g for about 22,000 shots during the 7th experimental campaign in 2003. In this campaign, the beam pulse width is 1 - 2 sec, the arc discharge duration is 7 - 8 sec, and the filament-on time is 17 - 18 sec for usual shots. In the 8th campaign in 2004, the ion source is modified for long-pulse operation with cooled PG, which is described in the next section, typical durations of the beam pulse, the arc discharge, and the filament-on time are 1 - 2 sec, 13 - 15 sec, and 23 - 25 sec, respectively. In this case, the Cs consumption was roughly estimated at 13 - 14 g for about 12,500 shots. The Cs consumption rate is much increased in the latter source. The Cs is supplied intermittently to maintain the negative ion intensity. In the latter source with the cooled PG, the pri-arc duration is extended to raise the PG temperature to the appropriate value for the negative ion production. Therefore, the extended arc discharge duration is considered to lead to the increase in the Cs consumption.

The filament lifetime determines the maintenance period of the ion source, and the filaments are replaced for 10,000 shots or more in the operational condition of the 7th campaign. The filament weight loss was measured in the 6th experimental campaign in 2002, and the total loss was around 2 g for 10,000 shots in the nearly the same operational condition as the 7the campaign [31]. The distribution of the filament weight loss seems to correspond to the arc distribution, suggesting that the evaporation of the tungsten filament is mainly related to the arc discharge. The filament replacement was carried out for around 5,000 shots in the long-pulse source with the cooled PG in the 8th campaign because an indication of the filament fatigue such as the snapping was observed. The arc discharge duration is increased nearly double in the long-pulse source, and this probably contributes to the reduction of the filament lifetime. Therefore, the enhancement of the Cs consumption in the long-pulse source is considered to be ascribed to the increase in the tungsten vapour. In the filament-arc discharge, the tungsten vapour would deteriorate the Cs effect as a dominant contaminant.

4. Long-Pulse and Steady-State Injection

The LHD negative-NBI system was originally designed for a maximum pulse length of 10 sec. By modification of the power supply system and the control system, the pulse length can be extended to over 10 min at a reduced power for two injectors. The main beamline components are designed for CW operation except for the injection port covered annually with inertially cooled molybdenum plates, which would limit the injection duration to a few minutes. The cryo-sorption pump can be operated for continuous gas load for 30 min. However, the ion source is optimized for the pulsed operation for several seconds with regard to the control of the PG temperature for the efficient negative ion production. That limits the present long-pulse operation in the LHD-NBI system.

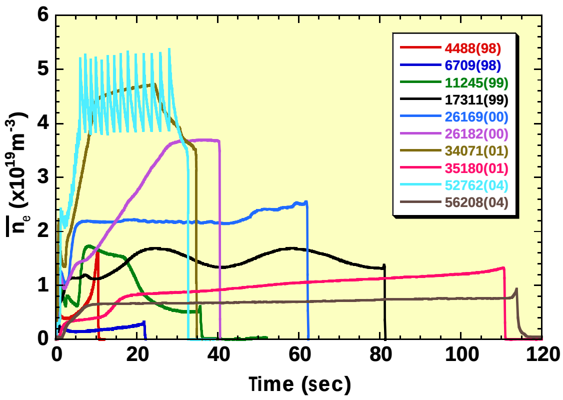

Fig. 12 Time evolutions of the plasma electron density for the long-pulse plasmas sustained by the NBI alone.

4.1 Extension of injection duration

In the LHD-NBI plasmas, the injection duration can be extended as long as the plasma is sustained by the NBI heating. Figure 12 shows examples of the long-pulse plasmas heated by the NBI alone, where the time variation of the plasma density is plotted as a function of the NB-injection time. The sustainable plasma density is determined by the injection power and the plasma purity. A high-density plasma of 4.5 x 10^{19} m^{-3} is sustained stationary for several tens of seconds with an injection power of 1.1 MW. With repetitive pellet injection a variable high-density plasma of (4 - 5) x 10^{19} m^{-3} is also sustained for 30 sec with an injection power of 1.2 MW. A long-pulse injection of 35 sec has been achieved with an injection power of 1.1 MW in every 10.5 min using one injector with two ion sources. The NBI operation utilizes usually a motor generator as an input power source, and the input power must be supplied directly from a commercial line to extend the injection duration to longer than 40 sec. In this case the injection power should be below 0.6 MW for avoiding the line distortion. With the commercial line, the injection duration is extended to around 80 sec with an injection power of around 0.5 MW, which sustains a plasma with a density of (1.5 - 2.0) x 10^{19} m^{-3} [23].

The beamline components are actively water-cooled, except for the molybdenum protection plates for the injection porthole. Although the temperature rise of the cooling water is nearly saturated in the above-mentioned injection condition, the water temperature starts occasionally to increase after the injection is past 1 min. Accordingly the injection power is gradually decreased, and then the LHD plasma is terminated with radiation collapse. The reduction of the injection power is caused by an excessive rise of the PG temperature. The PG temperature is monotonously increased during the arc discharge, and the negative ion current is decreased together with enlargement of the beam divergence when the PG temperature is increased to above about 350 ^{o}C. Therefore, the control of the PG temperature is a key issue for the long-pulse operation.

4.2 Direct cooling of PG

In order to suppress the PG temperature rise in the long-pulse operation, stainless-steel cooling tubes have been mechanically attached on the PG, as shown in Fig. 13. The thickness between the cooling channel and the contact surface is determined so that the heat diffusivity to the PG is lower than that of the molybdenum PG itself. By this structure, the distribution of the segmented PG temperature should be uniform. During the experimental campaign, most of plasma shots require a short pulse injection for 2 - 3 sec in every 3 min. Therefore, the thickness of the cooling tube should be selected as having such a heat removal capacity that the short-pulse operation is also possible by extending the pri-arc discharge duration before the beam extraction to around 15 sec from 5 - 7 sec in the case of no cooling tube. Figure 14 shows the PG temperature rise as a function of the arc discharge duration for the no-cooled PG and the cooled PG. While the PG temperature rise exceeds 200 ^{o}C at a discharge duration of about 80 sec for the no-cooled PG, the discharge duration is extended to about 160 sec for exceeding 200 ^{o}C of the PG temperature rise for nearly the same arc power of around 70 kW.

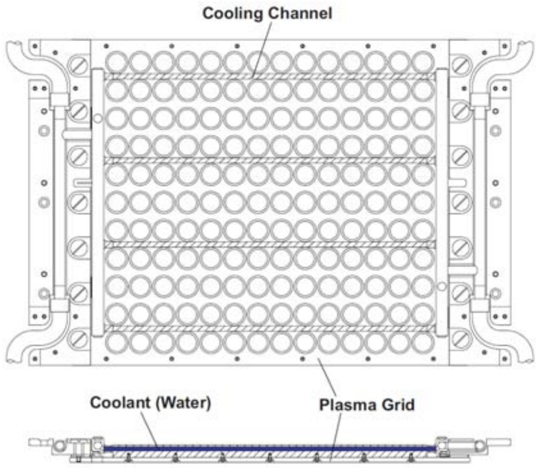

Fig. 13 Plan and side views of one part of the segmented plasma grid, on which the stainless-steel cooling channels are mechanically attached.

Using one ion source with the cooled PG, the injection duration was extended to above 120 sec with an injection power of 0.2–0.3 MW, and the injection was manually stopped due to the radiation collapse of the target plasma. The PG temperature rise was not saturated, and the injection duration would be limited to about 3 min in this case even if the plasma does not collapse. As the cooling rate of the PG after the injection is also larger with the cooled PG, a repetitive injection for several tens of seconds is also possible. In a long-pulse plasma lasting for 31 min and 45 sec, which was sustained with ICRF (ion cyclotron range of frequency) heating, the NB with a power of 0.5 MW was injected repetitively for 25 sec in every 3 min alternately with two ion sources (in every 6 min for each source). A series of 10 injections was successfully carried out in the long pulse plasma.

On the other hand, the longitudinal beam distribution is observed to be more uniform with the cooled PG than that with the previous thermally-insulated PG. An example of the vertical beam profile measured on the calorimeter 8.5 m downstream from the ion source is shown in Fig. 15. Although the arc discharge distribution is adjusted with the variable resistances of the individual output circuits of the arc power supply in this case, the similar vertical uniformity to that observed with the individual voltage control of the arc and filament power supplies as shown in Fig. 11. The temperature of the individual PG parts becomes more uniform with the cooled PG, which should contribute to the improvement of the beam uniformity.

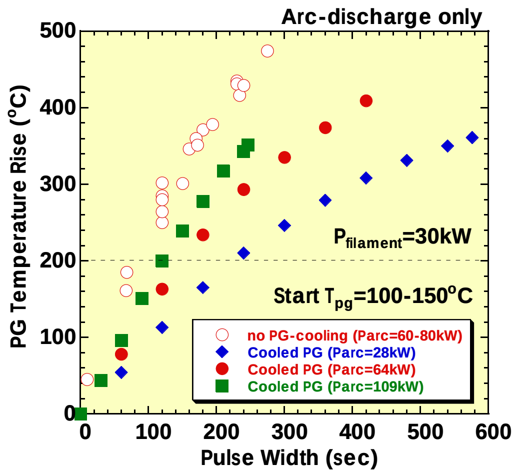

Fig. 14 PG temperature rise of the no-cooled PG and the cooled PG as a function of the pulse width of the arc discharge for various arc powers. The PG temperature at the start of the arc discharge is 100 - 150 ^{o}C.

With the cooled PG, however, the pri-arc duration must be extended to above 15 sec to maintain the appropriate PG temperature in the short pulse injection. This nearly doubled arc discharge duration leads to the reduction of the filament lifetime and the enhancement of the Cs consumption, as described in section 3.5. On the other hand, the PG cooling ability is not enough for the long-pulse injection, and the heat conductivity between the cooling channel and the PG should be much increased for the long-pulse injection towards the steady-state operation. This incompatibility for the PG cooling or thermal insulating structure between the long-pulse operation and the short-pulse operation is one of the present difficulties for the LHD negative-NBI operation.

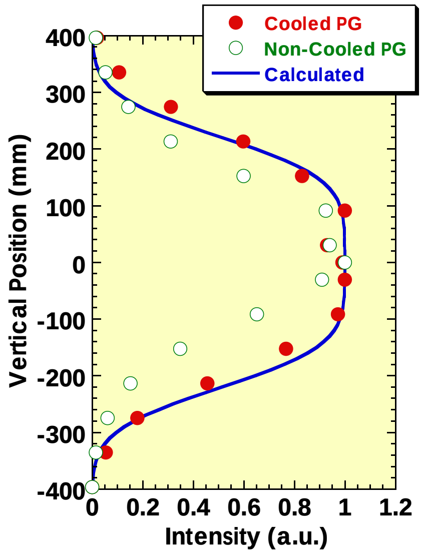

Fig. 15 Vertical beam profiles of measured on the calorimeter 8.5 m downstream from the ion source for the ion sources with the cooled PG and the no-cooled PG. The calculated profile for a uniform beam with a divergence angle of 10 mrad is also shown by a solid line in the figure.

5. Summary

Based on the 9 years' R&D, two negative-ion-based NB injectors with caesium-seeded negative ion sources were constructed in LHD, and started their operation in 1998. Including the third injector, which was operational in 2001, high-power injection has been carried out reliably in LHD, and the total injection power has been achieved to 13.1 MW. The negative-NBI operation is strongly dependent on the negative ion source performance. In the modified ion source with the multi-slotted GG, the beam energy is raised beyond the design value of 180 keV in a short conditioning period without serious breakdowns due to both reduction of the GG heat load and reduction of the gas pressure in the acceleration gap. Using the optimized arc chamber, in which the magnetic field configuration is optimized with regard to the primary electron distribution, the injection power is increased according to 5/2 power of the beam energy, and reaches 5.7 MW with an energy of 184 keV in one injector. The beam uniformity is improved with an individual control of the applied voltages of the arc and the filament power supplies, each output of which is divided into 12 circuits controlled independently. The maintenance period of the ion source is determined by the filament lifetime, and the weigh loss of the tungsten filaments has an influence on the caesium consumption. The tungsten vapour could be a dominant contaminant of the caesium.

The injection duration can be extended to several tens of seconds with a reduce power in two injectors. A long-pulse injection with a power of 1.1 MW is carried out repetitively in every 10.5 min using one injector. An excessive temperature rise of the PG, which leads to a degradation of the negative ion production, limits the long-pulse operation usually around 1 min. To mitigate the PG temperature rise during the long-pulse injection, stainless-steel cooling channels are mechanically attached on the PG. With the cooled PG, the PG temperature is increased more slowly, and the injection duration was extended to 120 sec with a beam power of 0.2–0.3 MW using one ion source. However, the incompatibility of the structure for the PG temperature control between the short-pulse operation and the long-pulse operation prevents the further long-pulse operation.

By continuing the improvement of the negative ion sources, the operational parameters such as the injection power and the injection duration would be enhanced in the LHD negative-NBI system, and these results should contribute to the development of the ITER negative-NBI system.

Acknowledgments

The authors acknowledge all the technical staff in LHD for their excellent operation of the LHD system. They are grateful to Prof. O. Motojima, Director-General, for his continuous encouragement and support. This work is partially supported by a Grant-in-Aid for Scientific Research of MEXT (Ministry of Education, Culture, Sports, Science and Technology) of Japan.

References

[1] R. S. Hemsworth, *et al.*, Rev. Sci. Instrum., **67** (1996) 1120.
[2] Y. Takeiri, *et al.*, Proc. 16th Symp. on Fusion Technology (London, 1990) Vol. 2, North-Holland, Amsterdam (1991) p. 1012.
[3] O. Kaneko, *et al.*, Proc. 17th Symp. on Fusion Technology (Rome, 1992) Vol. 1, North-Holland, Amsterdam (1993) p. 544.
[4] A. Ando, *et al.*, Phys. Plasmas **1** (1994) 2813.
[5] Y. Takeiri, *et al.*, Rev. Sci. Instrum., **66** (1995) 2541.
[6] Y. Takeiri, *et al.*, J. Plasma Fusion Res. **71** (1995) 605.
[7] K. Tsumori, *et al.*, Fusion Eng. Design **26** (1995) 473.
[8] Y. Takeiri, *et al.*, Rev. Sci. Instrum. **66** (1995) 5236.
[9] T. Kuroda, *et al.*, Rev. Sci. Instrum., **67** (1996) 1114.
[10] O. Kaneko, *et al.*, Proc. the 16th Inter. Conf. on Fusion Energy, (Montreal, 1996), IAEA, Vienna (1997), Vol. 3 p. 539.
[11] Y. Takeiri, *et al.*, Rev. Sci. Instrum. **68** (1997) 2003.
[12] Y. Oka, *et al.*, Rev. Sci. Instrum., **69** (1998) 920.
[13] Y. Takeiri, *et al.*, Rev. Sci. Instrum. **69** (1998) 977.
[14] Y. Takeiri, *et al.*, Rev. Sci. Instrum. **71** (2000) 1225.
[15] A. Iiyoshi, *et al.*, Nucl. Fusion **39** (1999) 1245.
[16] O. Kaneko, *et al.*, Nucl. Fusion, **43** (2003) 692.
[17] O. Motojima, *et al.*, Phys. Plasmas **6** (1999) 1843.
[18] M. Kuriyama, *et al.*, J. Nucl. Sci. Technol. **35** (1998) 739.
[19] K. Tsumori, *et al.*, Fusion Energy 2004 (Proc. 20th Int. Conf. Vilamoura, 2004) (Vienna: IAEA) CD-ROM file FT/1-2Rb.
[20] Y. Takeiri, *et al.*, Plasma Physics and Controlled Fusion **42** (2000) 147.
[21] T. Mutoh, *et al.*, Proc. 15th Symp. on Fusion Technology (Utrecht, 1988), North-Holland, Amsterdam (1989) p. 552.
[22] M. Osakabe, *et al.*, Rev. Sci. Instrum. **72** (2001) 590.
[23] Y. Takeiri, *et al.*, J. Plasma Fusion Res. SERIES, Vol. 3 (2000) 345.
[24] O. Motojima, *et al.*, Fusion Energy 2004 (Proc. 20th Int. Conf. Vilamoura, 2004) (Vienna: IAEA) CD-ROM file OV/1-5.
[25] O. Kaneko, *et al.*, Nucl. Fusion **39** (1999) 1087.
[26] K. Tsumori, *et al.*, Rev. Sci. Instrum., **75** (2004) 1847
[27] Y. Takeiri, *et al.*, J. Plasma Fusion Res. **74** (1998) 1434.
[28] M. Hamabe, *et al.*, Rev. Sci. Instrum. **72** (2001) 3237.
[29] Y. Takeiri, *et al.*, Rev. Sci. Instrum. **73** (2002) 1087.
[30] K. Ikeda, *et al.*, Rev. Sci. Instrum., **75** (2004) 1744.
[31] Y. Oka, *et al.*, Rev. Sci. Instrum., **75** (2004) 1803.